Efficient crosswell EM tomography using localized nonlinear approximation

Hee Joon Kim[1], Yoonho Song[2], Ki Ha Lee[3], and Michael J. Wilt[4]

Key Words: crosswell, LN approximation, electromagnetic, cylindrical symmetry, inversion

ABSTRACT

This paper presents a fast and stable imaging scheme using the localized nonlinear (LN) approximation of integral equation (IE) solutions for inverting electromagnetic data obtained in a crosswell survey. The medium is assumed to be cylindrically symmetric about a source borehole and to maintain the symmetry a vertical magnetic dipole is used as a source. To find an optimum balance between data fitting and smoothness constraint, we introduce an automatic selection scheme of Lagrange multiplier, which is sought at each iteration with a least misfit criterion. In this selection scheme, the IE algorithm is quite attractive in speed because Green's functions, a most time-consuming part in IE methods, are repeatedly re-usable throughout the inversion process. The inversion scheme using the LN approximation has been tested to show its stability and efficiency using both synthetic and field data. The inverted image derived from the field data, collected in a pilot experiment of water flood monitoring in an oil field, is successfully compared with that of a 2.5-dimensional inversion scheme..

---

1 Department of Environmental Exploration Engineering,
Pukyong National University,
Busan 608-737, Korea
Email: hejkim@pknu.ac.kr

2 Korea Institute of Geoscience & Mineral Resources,
Daejeon 305-350, Korea
Email: song@kigam.re.kr

3 Earnest Orlando Lawrence Berkeley National Laboratory,
Berkeley, CA 94720, U.S.A.
Email: KHLee@lbl.gov

4 ElectroMagnetic Instruments, Inc.,
Richmond, CA 94804, U.S.A.
Email: wilt@emiinc.com

INTRODUCTION

High-resolution imaging of electrical conductivity has been the subject of many studies in crosswell tomography using electromagnetic (EM) fields (Zhou et al., 1993; Wilt et al., 1995; Alumbaugh and Morrison, 1995; Newman, 1995; Alumbaugh and Newman, 1997). Although the theoretical understanding and associated field practices for crosswell EM methods are relatively mature, fast and stable inversion of crosswell EM data is still a challenging problem.

Since Raiche (1974) first formulated a three-dimensional (3-D) volume integral equation (IE) method, many numerical solutions have been presented on this subject (Hohmann, 1988). The main advantage of IE method over the finite difference (FD) and/or finite-element (FE) methods is its greater suitability for inversion. For example, IE formulation readily contains a sensitivity matrix, which can be revised at each inversion iteration at little expense. With the FD or FE method, in contrast, the sensitivity matrix has to be recomputed at each iteration at a cost nearly equal to that of full forward modeling. The IE method, however, has to overcome a severe practical limitation imposed on the size of imaging domain for inversion purposes. In this direction, several approximate methods such as localized nonlinear (LN) approximation (Habashy et al., 1993) and quasi-linear approximation (Zhdanov and Fang, 1996) have been developed. Recently, Lee et al. (2002) applied the LN approximation for a cylindrically symmetric model to inverting single-hole EM data.

In this paper an advantage of the LN approximation of cylindrically symmetric IE solution is further exploited with applications to crosswell EM tomography. We begin our discussion with a critical check of the accuracy of LN approximation for a cylindrically symmetric model. We then describe our EM inversion algorithm and demonstrate its stability and effectiveness by inverting synthetic data. Finally, we present an example application to field data obtained as a part of pilot project of water flood monitoring at the Lost Hills oil field in central California, U. S. A.

LN APPROXIMATION

The LN approximation of IE solutions for a cylindrically symmetric model is described in detail in Lee et al. (2002). For completeness, the algorithm is briefly outlined here.

Assuming an $e^{+i\omega t}$ time dependency and neglecting displacement currents, an IE solution for the electric field $\mathbf{E}(\mathbf{r})$ at $\mathbf{r}$ can be written by (Hohmann, 1975)

$$\mathbf{E}(\mathbf{r}) = \mathbf{E}_b(\mathbf{r}) - i\omega\mu \int_V \mathbf{G}_E(\mathbf{r}-\mathbf{r}') \cdot \Delta\sigma(\mathbf{r}')\mathbf{E}(\mathbf{r}')dv', \qquad (1)$$

where $\mathbf{E}_b(\mathbf{r})$ is the background electric field, $\mathbf{G}_E(\mathbf{r}\text{-}\mathbf{r}')$ the electric Green's tensor, σ the electrical conductivity, ω the angular frequency, and μ the magnetic permeability. In equation (1), $\Delta\sigma(\mathbf{r}')$ inside the integral means the excess conductivity, $\sigma(\mathbf{r}') - \sigma_b$, and the term $\Delta\sigma\mathbf{E}$ is called the scattering current (Hohmann, 1975). Each vector component of the Green tensor

$\mathbf{G}_E(\mathbf{r}\text{-}\mathbf{r}')$ is the vector electric field at $\mathbf{r}$ due to a point source at $\mathbf{r}'$ with its current density of $(-i\omega\mu)^{-1}$ A/m^2, polarized in x, y, and z, respectively. To obtain a numerical solution of equation (1), the anomalous body is first divided into a number of cubic cells, and a constant electric field is assigned to each cell (Hohmann, 1988). The process involved in volume IE methods requires computing time proportional to the cubic of the number of cells used, and it quickly becomes impractical as the size of inhomogeneity is increased to handle realistic problems.

The complexity associated with a full 3-D problem can be greatly reduced for a model whose conductivity is cylindrically symmetric in the vicinity of a borehole. In order to preserve the cylindrical symmetry in the resultant EM fields, a horizontal loop current or a vertical magnetic dipole may be considered as a source in the borehole. When the problem is formulated using an azimuthal electric field E_φ, which is scalar, the resultant IE solution is

$$E_\varphi(\mathbf{r}) = E_{\varphi b}(\mathbf{r}) - 2\pi i\omega\mu \iint_{\rho z} G_E(\mathbf{r}-\mathbf{r}')\Delta\sigma(\mathbf{r}')E_\varphi(\mathbf{r}')\rho' d\rho' dz', \tag{2}$$

where $\mathbf{r} = \vec{\rho} + \vec{z}$ and $\mathbf{r}' = \vec{\rho}' + \vec{z}'$ are the position vectors. The Green's function, which is also scalar, is given in the form of a Hankel transform as (Ward and Hohmann, 1988, p. 219)

$$G_E(\rho, \rho'; z-z') = -\frac{1}{4\pi}\int_0^\infty \frac{e^{-u_b|z-z'|}}{u_b}\lambda J_1(\lambda\rho)J_1(\lambda\rho')d\lambda, \tag{3}$$

where $u_b = (\lambda^2 + i\omega\mu\sigma_b)^{1/2}$ is the vertical wave number and J_1 is the Bessel function of order 1. Since measurements are usually made for vertical magnetic fields, equation (2) is modified as

$$H_z(\mathbf{r}) = H_{zb}(\mathbf{r}) - 2\pi i\omega\mu \iint_{\rho z} G_H(\mathbf{r}-\mathbf{r}')\Delta\sigma(\mathbf{r}')E_\varphi(\mathbf{r}')\rho' d\rho' dz', \tag{4}$$

where $G_H(\mathbf{r}\text{-}\mathbf{r}')$ is the magnetic Green's function, which translates the scattering current $\Delta\sigma(\mathbf{r}')E_\varphi(\mathbf{r}')$ at $\mathbf{r}'$ to the magnetic field at $\mathbf{r}$. The magnetic Green's function can be deduced from the corresponding electric one (3) as

$$G_H(\rho, \rho'; z-z') = \frac{1}{4\pi i\omega\mu}\int_0^\infty \frac{e^{-u_b|z-z'|}}{u_b}\lambda^2 J_0(\lambda\rho)J_1(\lambda\rho')d\lambda. \tag{5}$$

Using equations (2) through (5), we can obtain an IE solution by first dividing the (ρ, z) cross-section into a number of cells, and formulate a system of equations for the electric field using a pulse basis function.

The LN approximation offers an efficient and reasonably accurate electric-field solution (Habashy et al., 1993). For the problem where there is only the azimuthal electric field, a good approximation to equation (2) is given by (Lee et al., 2002)

$$E_\varphi(\mathbf{r}) \approx \gamma(\mathbf{r})E_{\varphi b}(\mathbf{r}), \tag{6}$$

where

$$\gamma(\mathbf{r}) = \left[1 + 2\pi i \omega \mu \iint\limits_{\rho z} G_E(\mathbf{r} - \mathbf{r}') \Delta\sigma(\mathbf{r}') \rho' d\rho' dz' \right]^{-1}.$$

Substituting equation (6) into equation (4) yields an approximate magnetic-field solution

$$H_z(\mathbf{r}) \approx H_{zb}(\mathbf{r}) - 2\pi i \omega \mu \iint\limits_{\rho z} G_H(\mathbf{r} - \mathbf{r}') \Delta\sigma(\mathbf{r}') \gamma(\mathbf{r}') E_{\varphi b}(\mathbf{r}') \rho' d\rho' dz' . \tag{7}$$

Upon dividing the inhomogeneity into K elements, the secondary magnetic field at the i-th receiver may be written as

$$H_{zi}^s \approx -2\pi i \omega \mu \sum_{k=1}^{K} \Delta\sigma_k \gamma_k E_{\varphi bk} \iint\limits_{S_k} G_H(\rho_i, \rho', z_i - z') \rho' d\rho' dz', \tag{8}$$

where subscript k denotes the k-th element.

To demonstrate the efficiency and usefulness of LN solutions in a crosswell application, let us consider a simple model consisting of a conductive ring about a source borehole axis in a uniform whole space of 100 Ω-m. The cross-section of the ring is a 10 m by 10 m rectangle and horizontally 15 m away from the borehole as shown in Figure 1. Born and LN approximated magnetic fields measured in the other borehole 50 m away from the source borehole are compared with results obtained from a FE method (Lee et al., 2003).

Figure 2 shows the comparison in secondary vertical magnetic fields between Born, LN, and FE solutions. The center of the body is chosen as $z = 0$. The conductivity contrast and operating frequency used are 10 and 10 kHz, respectively. The source and receiver are located at the same depth in each borehole. Stronger anomalies can be observed in the imaginary part than in the real part and the LN and FE solutions agree very well.

We are also interested in the quality of LN solutions when the conductivity of the body varies. Figure 3 shows the comparison in secondary vertical magnetic fields between Born, LN, and FE solutions. A vertical magnetic dipole source is fixed at the depth of the center of body in the source borehole, and vertical magnetic fields are measured at 10 m below the center of the body in the receiver borehole. The frequency used is 10 kHz. The LN approximation works very well up to the conductivity contrast of about 100. The imaginary part of the LN solution starts deviating from the FE solution beyond the conductivity contrast of 100, while the real part still shows a good agreement.

Finally, a comparison is made for responses in frequency as shown in Figure 4. The source-receiver array is the same as that in Figure 3, and the conductivity contrast is fixed to 10. The LN and FE solutions show a good agreement all the way up to about 100 kHz. From these forward solutions we can conclude that the LN approximation has sufficient accuracy for a practical application.

CROSSWELL TOMOGRAPHY

Based on the encouraging results on the LN approximation as described above, we have proceeded to implement crosswell EM inversion scheme. For the inversion, the sensitivity of the magnetic field with respect to the change in conductivity can be easily obtained from equation (8). Taking derivative of the magnetic field with respect to the *j*-th conductivity parameter and neglecting the dependence of γ_j on $\Delta\sigma_j$, the sensitivity becomes

$$\frac{\partial H_{zi}^{s}}{\partial \sigma_j} \approx -2\pi i\omega\mu\gamma_j E_{\varphi bj} \iint_{S_j} G_H(\rho_i, \rho', z_i - z')\rho' d\rho' dz', \tag{9}$$

which can be easily evaluated by integrating the magnetic Green's function over the area of *j*-th cell.

The inversion procedure starts with the data misfit $\|\mathbf{W}_d[\mathbf{H}(\sigma)\text{-}\mathbf{H}_d]\|^2$, where $\|\bullet\|^2$ denotes the L2 norm, $\mathbf{W}_d$ is the data weighting matrix and subscript *d* represents data. If a perturbation $\delta\sigma$ is allowed to the conductivity, the misfit takes a form $\|\mathbf{W}_d[\mathbf{H}(\sigma+\delta\sigma)\text{-}\mathbf{H}_d]\|^2$, and a total objective functional can be written as

$$\phi = \left\|\mathbf{W}_d[\mathbf{H}(\sigma+\delta\sigma) - \mathbf{H}_d]\right\|^2 + \lambda\left\|\mathbf{W}_\sigma \delta\sigma\right\|^2, \tag{10}$$

where the second term on the right-hand side is added to impose a smoothness constraint, $\mathbf{W}_\sigma$ is the weighting matrix for σ, and λ is the Lagrange multiplier that controls the trade-off between data misfit and parameter smoothness. Expanding the misfit in $\delta\sigma$ using the Taylor series, discarding terms higher than the second-order term, and letting the variation of the functional with respect to $\delta\sigma$ equal to zero, we can obtain a linear system of normal equations for the perturbation $\delta\sigma$ as

$$(\mathbf{J}^T\mathbf{W}_d^T\mathbf{W}_d\mathbf{J} + \lambda\mathbf{W}_\sigma^T\mathbf{W}_\sigma)\delta\sigma = -\mathbf{J}^T\mathbf{W}_d^T\mathbf{W}_d[\mathbf{H}(\sigma) - \mathbf{H}_d], \tag{11}$$

where superscript *T* indicates the matrix transpose, and the entries of Jacobian matrix **J** are the sensitivity functions given in equation (9).

The stability of inversion is largely controlled by requiring the conductivity to vary smoothly. Larger values of λ result in smooth and stable solutions at the expense of resolution. It even allows for the solution of grossly underdetermined problems (Tikhonov and Arsenin, 1977). In this crosswell tomography, we employ the Occam approach, first proposed by Constable et al. (1987) (see also deGroot-Hedlin and Constable, 1990; Parker, 1994), to determine an optimum λ during the inversion process. The unique feature of the Occam approach is that the parameter λ is used at each iteration both as a step length control and as a smoothing parameter. That is, equation (11) is solved for a series of trial values of λ and the rms misfit for each λ is evaluated by solving the 2-D forward problem. The Occam process thus chooses the model with minimum misfit as the basis for the next iteration. The minimization can be carried out by means of a simple 1-D line search. In this selection scheme, IE modeling is quite attractive in speed because Green's functions for the electric field involving the Hankel transform, the most time-consuming part in IE methods, are repeatedly re-usable throughout the selection procedure. In this study forward modeling is conducted

three times to select an optimum λ at each iteration.

To evaluate the performance of crosswell tomography using the LN approximation, we choose a conductivity model shown in Figure 5. The model consists of two cylindrically symmetric bodies, one conductive (0.1 S/m) and the other resistive (0.001 S/m), in a whole space of 0.01 S/m. A FE scheme (Lee et al., 2003) is used to generate synthetic data. Using a vertical magnetic dipole (M_z) as a source, vertical magnetic fields (H_z) are computed at three frequencies of 2.5 kHz, 10 kHz and 20 kHz. Three-percent Gaussian noise is added to the synthetic data prior to the inversion. The inversion is started with an initial model of 60 Ω-m uniform whole space.

After 7 iterations, the two bodies are clearly reconstructed as shown in Figure 6. The recovered conductivity is found to be nearly the same in the conductive body but is overestimated in the resistive body. The inversion process is quite stable and the rms misfit decreases from the initial guess of 5.095 to 0.032 after 7 iterations (Figure 7). The smoothing parameter varies significantly during the inversion process. This means it is difficult to determine the parameter a priori.

Finally, our inversion algorithm has been applied to a set of crosswell EM data collected as a part of water flood monitoring at the Lost Hills oil field in central California (Wilt et al., 2001). Two fiberglass cased wells were installed at the southern margin of the oil field for the monitoring and the separation between these two observation wells was 82 m. Although EM data for the pre- and post-injection of water are available, we analyze only the pre-injection EM (M_z-H_z) data. The operating frequency was 1,000 Hz.

A 2-D inversion result is shown in Figure 8 along with a 2.5-D inversion result for comparison. The 2.5-D inversion scheme also uses the LN approximation for both forward and sensitivity calculations (Song et al., 2001). The cell size for these images is 5 × 5 m. Initial model used is 1.4 ohm-m uniform whole space and after 5 iterations the rms misfit is reduced to about 7 % (Figure 9). Both methods give similar images for different model dimensions. The resistive (1.5 – 2 ohm-m) zone shallower than 760 m is considered as the chief oil bearing zone at the field (Wilt et al., 2001). Alumbaugh and Morrison (1995) showed that the effects of structures outside of the interwell plane are minimized for borehole separations greater than five skin depths. Since the minimum separation between source and receiver in our case is about 4.5 times greater than the skin depth (about 19 m), reconstructed images thus may have few artifacts and the approximation of 2-D cylindrical geometry can provide similar results to those other schemes at much less computational cost. Computing time required for this 2-D approximate inversion is only less than 5 minutes to obtain 588 conductivities from 1368 complex H_z data on a Pentium IV, 1.5 GHz processor with 512 MB of RAM, compared to about 2 days for the 2.5-D inversion.

CONCLUSIONS

The LN approximation of IE solutions has been applied to inverting crosswell EM data using a cylindrically symmetric model. When the LN approximation is applied to the cylindrically symmetric model with a vertical magnetic dipole source, it works very well because electric fields are scalar and continuous everywhere. One of the most important steps in the inversion is the selection of a proper regularization parameter for stability. The LN

solution provides an efficient means for selecting an optimum regularization parameter, because Green's functions, the most time-consuming part in IE methods, are repeatedly re-usable at each iteration. This fast imaging scheme has been tested on its stability and efficiency using both synthetic and field data. The reconstructed image from the field data, obtained in a pilot study for water flood monitoring at the Lost Hills oil field, is successfully compared with that of the 2.5-D inversion scheme.

ACKNOWLEDGEMENTS

Korea Science and Engineering Foundation (R01-2001-000-000071-0) provided support for this study. The second author's (Y. Song) work was supported by the Korean Ministry of Science and Technology through National Research Lab. Funding. The third author (K. H. Lee) is a collaborator whose work was partially supported by the Assistant Secretary for Energy Efficiency and Renewable Energy, Office of Wind and Geothermal Technologies of the U.S. Department of Energy under Contract No. DE-AC03-76SF00098

REFERENCES

Alumbaugh, D.L. and Morrison, H.F., 1995, Theoretical and practical considerations for crosswell electromagnetic tomography assuming a cylindrical geometry: *Geophysics*, **60**, 846-870.

Alumbaugh, D.L., and Newman, G.A., 1997, Three-dimensional massively parallel electromagnetic inversion— II. Analysis of crosswell electromagnetic experiment: *Geophys. J. Int*., **128**, 355-363.

Constable, S.C., Parker, R.L., and Constable, C.G., 1987, A practical algorithm for generating smooth models from electromagnetic sounding data: *Geophysics*, **52**, 289-300.

deGroot-Hedlin, C., and Constable, S.C., 1990, Occam's inversion to generate smooth, two-dimensional models from magnetotelluric data: Geophysics, **55**, 1613-1624.

Habashy, T.M., Groom, R.M., and Spies, B.R., 1993, Beyond the Born and Rytov approximations: a nonlinear approach to electromagnetic scattering: *J. Geophys. Res*., **98**, 1795-1775.

Hohmann, G.W., 1975, Three-dimensional induced polarization and EM modeling: *Geophysics*, **40**, 309-324.

Hohmann, G.W., 1988, Numerical modeling for electromagnetic methods of geophysics, *in* Nabighian, M.N., Ed., Electromagnetic Methods in Applied Geophysics, Vol. 1, Soc. Expl. Geophys., 313-363.

Lee, K.H., Kim, H.J., and Uchida, T., 2003, Electromagnetic fields in steel-cased borehole: *Geophys. Prosp*. (submitted)

Lee, K.H., Kim, H.J., and Wilt, M., 2002, Efficient imaging of single-hole electromagnetic data: *Geothermal Resources Council Transactions*, **26**, 399-404.

Newman, G.A., 1995, Crosswell electromagnetic inversion using integral and differential equations: *Geophysics*, **60**, 899-911.

Parker, R.L., 1994, Geophysical Inverse Theory, Prinston Univ. Press.

Raiche, A.P., 1974, An integral equation approach to 3D modeling: *Geophys. J. Roy. astr. Soc.*, **36**, 363-376.

Song, Y., Kim, J.-H., and Chung, S.-H., 2001, An efficient 2.5-D inversion of loop-loop EM data, Proc. 5th SEGJ Int. Symp., 153-160.

Tikhonov, A.N., and Arsenin, V.Y., 1977, Solutions to Ill-Posed Problems, John Wiley and Sons, Inc.

Ward, S.H., and Hohmann, G.W., 1988, Electromagnetic theory for geophysical applications, *in* Nabighian, M.N., Ed., Electromagnetic Methods in Applied Geophysics, Vol. 1, Soc. Expl. Geophys., 131-311.

Wilt, M.J., Alumbaugh, D.L., Morrison, H.F., Becker, A., Lee, K.H., and Deszcz-Pan, M., 1995, Crosshole electromagnetic tomography: System design considerations and field results: *Geophysics*, **60**, 871-885.

Wilt, M.J., Zhang, P., Osato, K., and Tsuneyama, F., 2001, Crosswell EM studies at the Ellis Lease, Lost Hills California, Proc. 5th SEGJ Int. Symp., 243-250.

Zhdanov, M.S., and Fang, S., 1996, Quasi-linear approximation in 3-D EM modeling: *Geophysics*, **61**, 646-665.

Zhou, Q., Becker, A., and Morrison, H.F., 1993, Audio-frequency electromagnetic tomography in 2-D: *Geophysics*, **58**, 482-495.

Figure Captions

Fig. 1. A cylindrically symmetric model. A conductive body with a cross-section of 10 m by 10 m is cylindrically symmetric about a source borehole in which a vertical magnetic dipole source is inserted, and located horizontally 15 m away from the source borehole in a whole space of 0.01 S/m. Magnetic fields are measured in the other borehole 50 m horizontally away from the source borehole.

Fig. 2. Vertical components of secondary magnetic fields. The operating frequency is 10 kHz and the conductivity of the body is 0.1 S/m. The array used is a crosswell source-receiver pair keeping the same depth in each borehole. The solid and dashed lines show FE solutions.

Fig. 3. The effect of conductivity contrast between the body and background on the vertical components of secondary magnetic fields. The depths of source and receiver are fixed at 5 m above and below the bottom of the body, respectively. The operating frequency is 10 kHz. The solid and dashed lines show FE solutions.

Fig. 4. The effect of frequency on the vertical components of secondary magnetic fields. The depths of source and receiver are fixed at 5 m above and below the bottom of the body, respectively. The conductivity of the body is 0.1 S/m.

Fig. 5. A model used to calculate synthetic data for inversion test. Two rings of 0.1 S/m and 0.001 S/m, separated vertically by 10 m, are located in a whole-space of 0.01 S/m. The upper and lower bodies are at horizontally 10 m and 30 m away from the source borehole, respectively.

Fig. 6. An image of the two bodies reconstructed from the inversion of synthetic data after 7 iterations.

Fig. 7. Convergence in rms misfit and associated Lagrange multiplier as a function of iteration during the synthetic model inversion.

Fig. 8. Comparison of resistivity images derived from the 2-D (a) and 2.5-D (b) inversion of crosswell EM data collected at the Lost Hills oil field in central California. The pixel size for these images is 5×5 m and the initial model is a homogeneous whole space of 1.4 ohm-m.

Fig. 9. Convergence of rms misfits during the 2-D and 2.5-D inversion of crosswell EM data collected at the Lost Hills oil field in central California.

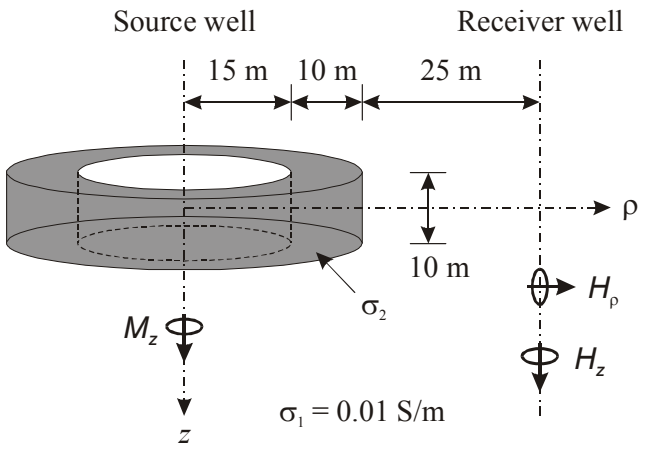

Fig. 1. (5.5 cm wide)

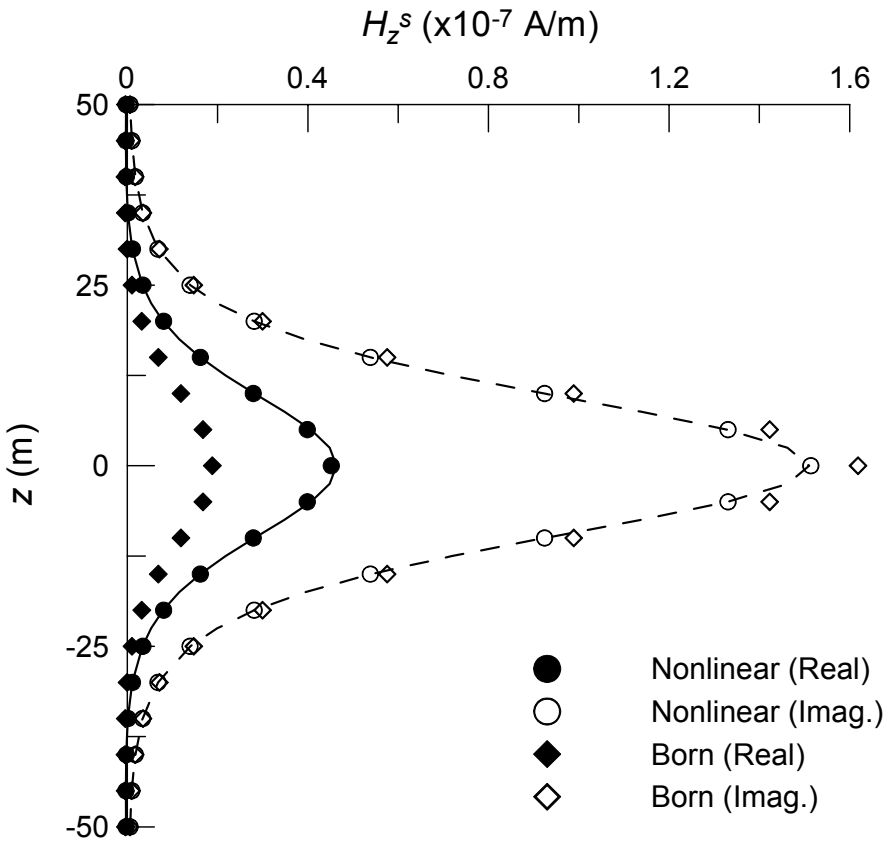

Fig. 2. (5.5 cm wide)

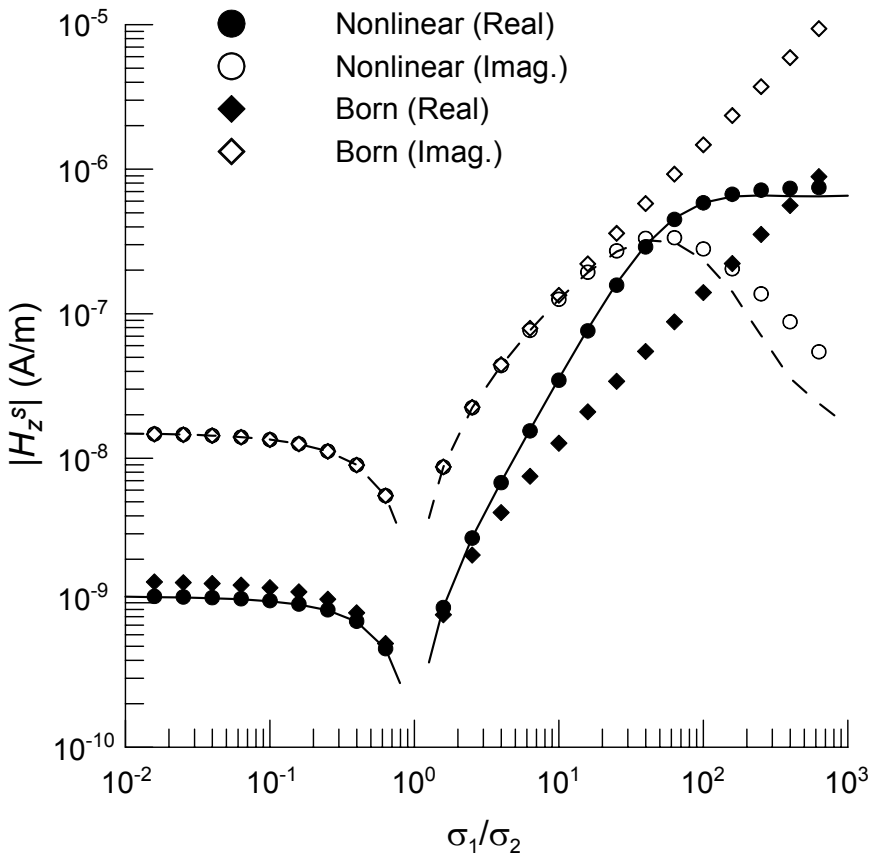

Fig. 3. (5.5 cm wide)

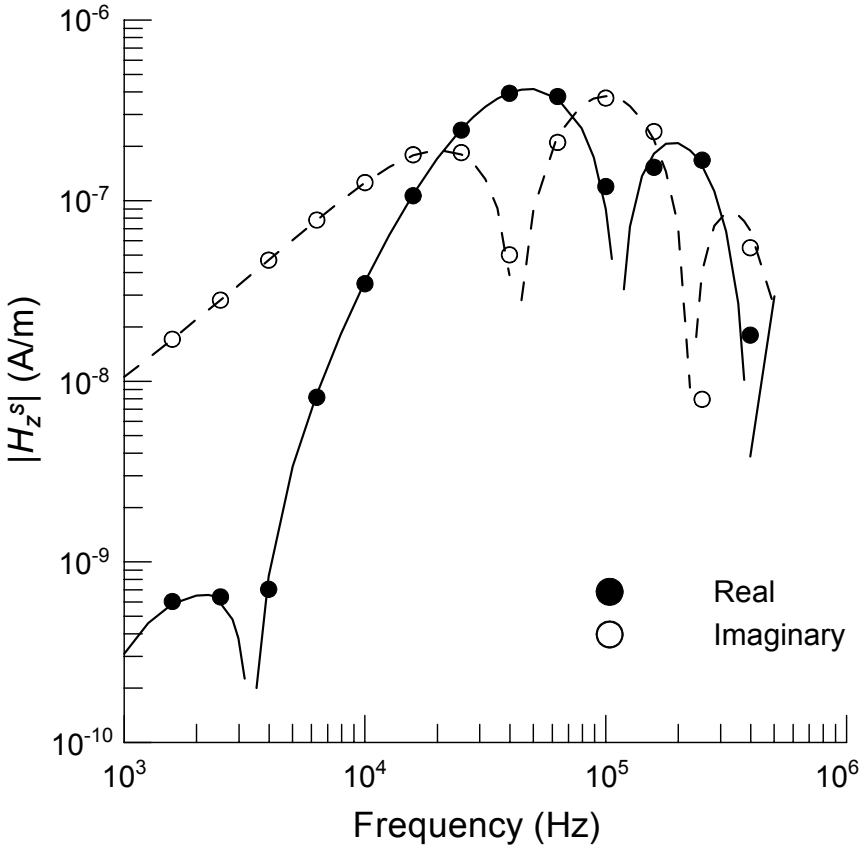

Fig. 4. (5.5 cm wide)

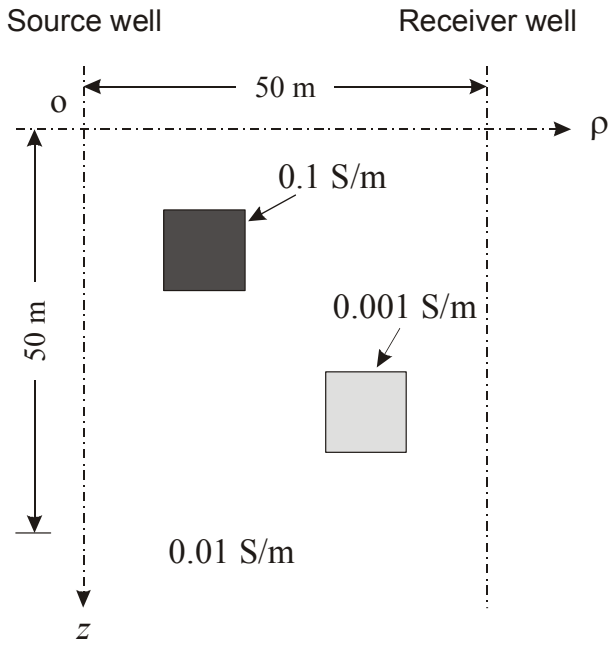

Fig. 5. (5 cm wide)

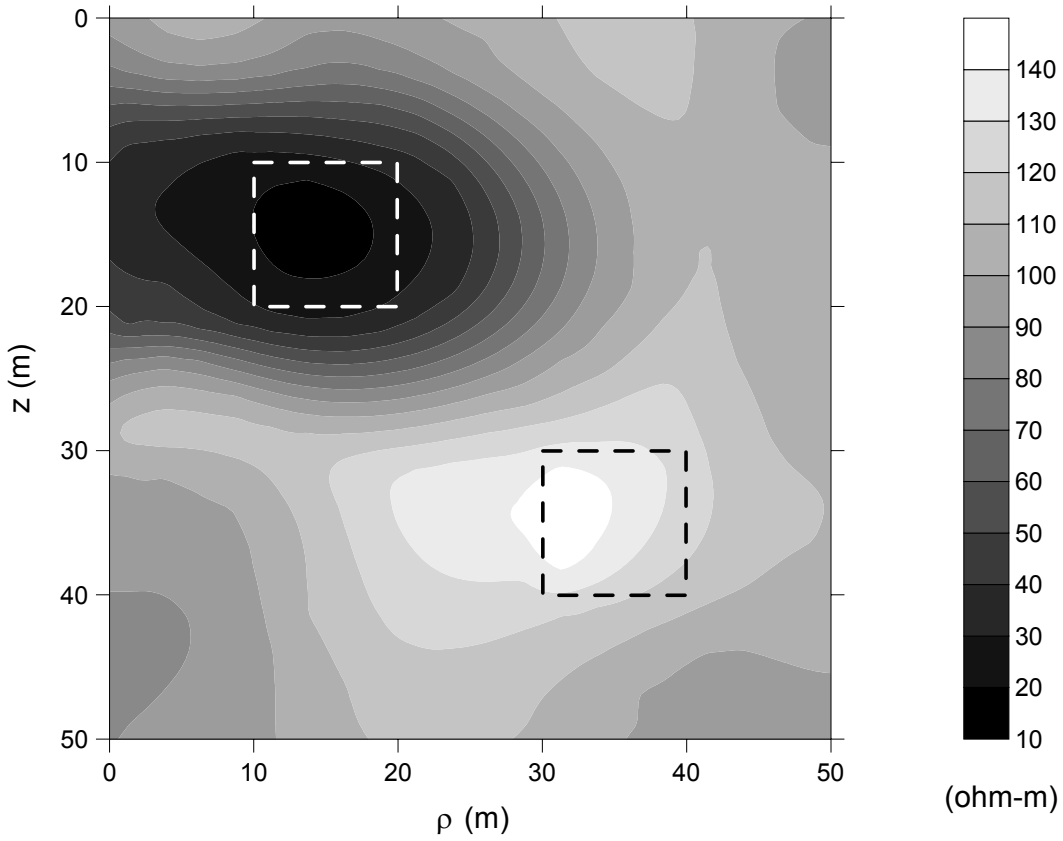

Fig. 6. (6 cm wide)

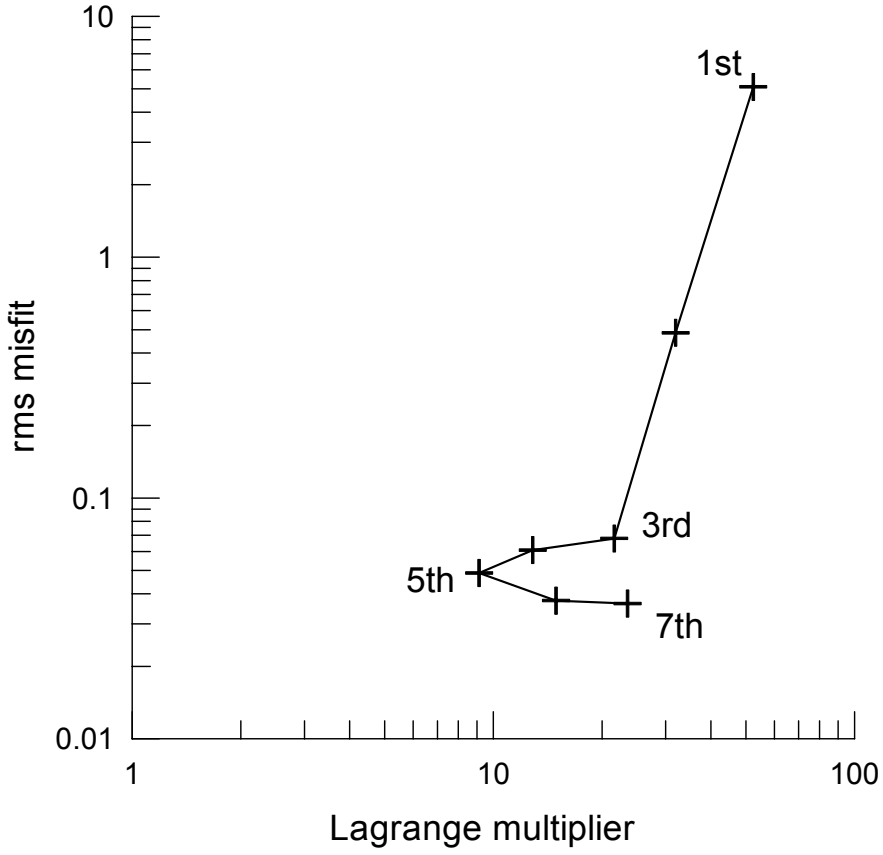

Fig. 7. (5.5 cm wide)

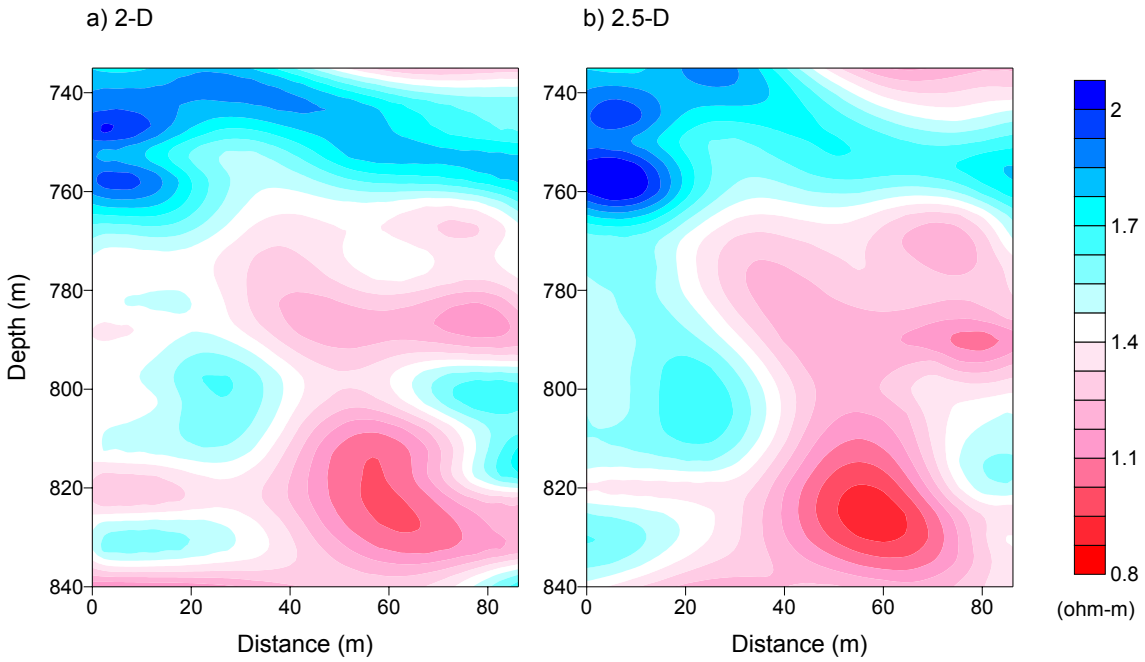

Fig. 8. (7 cm wide)

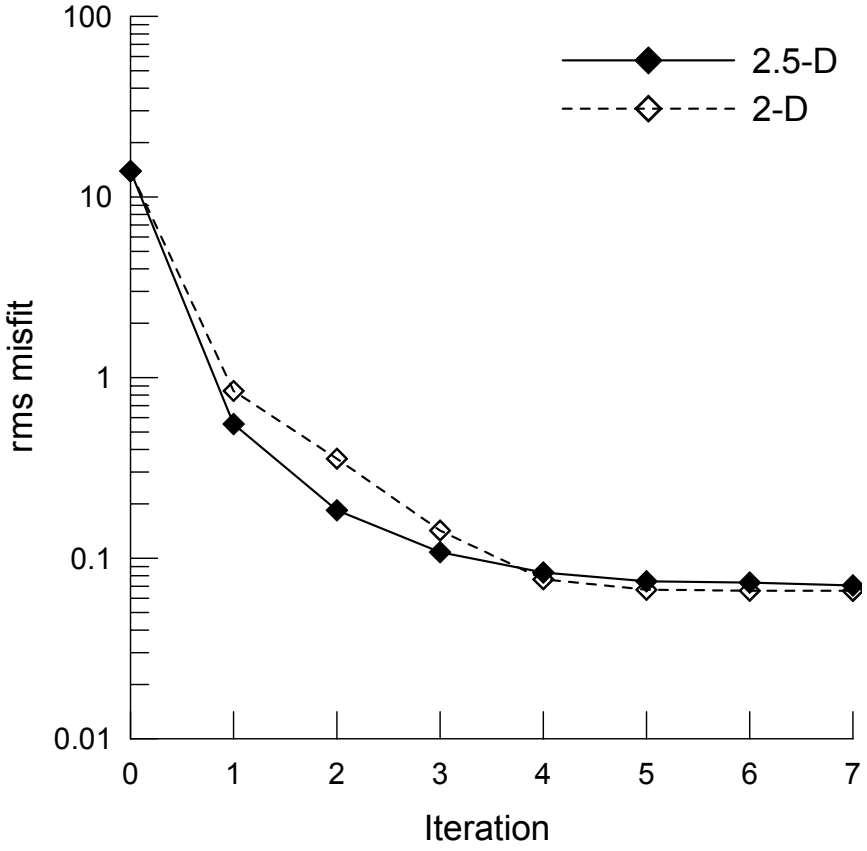

Fig. 9. (5.5 cm wide)